Check for updates

ACES Asian Chemical Editorial Society

doi.org/10.1002/cnma.202200237

CHEMNANOMAT
Research Article

www.chemnanomat.org

Hierarchical TS-1 Through Ammonium Fluoride Etching

Thilali Akkal,[a, b] Ahcène Soualah,[a] Sophie Morisset,[b] Julie Rousseau,[b] Nourrdine Chaouati,[a] and Alexander Sachse*[b]

Abstract: The impact of the NH_4F etching on the textural and catalytic properties of TS-1 was investigated. Two TS-1 with different crystal sizes, i.e. 200 and 100 nm; were achieved, with different textural properties as inferred from nitrogen physisorption isotherms at 77 K, mercury porosimetry, powder X-ray diffraction patterns and transmission electron microscopy. The generation of larger mesopores within the parent samples was observed together with a reduction of the coherent crystal size (CCS) upon NH_4F etching. The generation of secondary porosity further did not result in an alteration of the Si/Ti ratio, allowing to compare the catalytic outcomes of the samples as a function of the textural properties. It was found that the methyl-phenyl sulfide (MPS) conversion kinetics importantly depend on the textural properties of the catalysts. The initial velocity was found to increase linearly with the reduction of the CCS until reaching a plateau, indicating that diffusion limitation occur up to a CCS of approximately 100 nm. Likewise, mono- and di-oxidation product selectivity was governed by diffusion issues.

Introduction

Zeolites present unique textural and chemical properties, which make them very valuable in a number of industrial applications including, catalysis, separation and adsorption. Yet, zeolites have been described to be victims of their own success, as the sole presence of micropores imposes diffusions limitations, which might severely impact catalytic outputs.[1] Long diffusion path lengths indeed often reduce catalytic activity and selectivity by favoring the occurrence of secondary reactions.[2,3] These might further negatively impact catalyst stability, as the extended micropore system reduces importantly diffusion of bulky molecules to and from the active sites.[4] The diffusion path length is proportional to the Thiele modulus. This latter is inversely proportional to the catalytic effectiveness factor. Long diffusion path lengths favor low effectiveness factors. Hence, only a fraction of the active sites are used in the catalytic process.

In order to reduce these limitations, the reduction of the diffusion path length is a sound solution, which can be achieved by three approaches, i.e. the downsizing of the crystal size of zeolites the development of bidimensional zeolites or the development of hierarchical zeolites. Some approaches have been published on the development of nanosized zeolites (<100 nm) using microwave heating and ultrananosized zeolites (<20 nm). Yet, these methods often feature the inconvenience of low incorporation of Ti into the zeolite framework and low yields.[3,5,6] The achievement of bidimensional zeolites often requires the use of expensive organosilanes.[7] As far as hierarchical zeolites are concerned increased research efforts have been made since the beginning of the present century for the development and optimization of various strategies.[8] These can be classified as constructive or destructive approaches. The latter is realized through a post-synthetic treatment of a given zeolite, which allows to generate secondary porosity within the crystals. Due to the cost efficiency of many of these post-synthetic strategies they emerge as most viable solutions for possible industrial applications.[9] The most prominent strategies are based on dealumination and desilication treatments that allow through the use of water vapor, acid or alkaline treatments to partially destroy the zeolite framework, hence allowing for the generation of mesopores.[10]

Rather recently Valtchev and co-workers proposed a new post-synthetic treatment based on the etching of zeolites with aqueous NH_4F solution.[11,12] It has been speculated that through the hydrolysis of NH_4F a highly active species, i.e. HF_2^-, generates allowing for the unbiased leaching of Si and Al from the zeolite framework, and preferentially attacks structural defect zones in the zeolite crystals. This etching procedure has been put forward as promising strategy as it allows to reduce the impact on the overall zeolite acidity upon hierarchization.

The isomorphic substitution of aluminum of the zeolite framework with heteroatoms leads to so-called zeotypes.[13] One famous example is the introduction of titanium in the MFI structure resulting to the well-known titanosilicalite-1 (TS-1),[14] which revealed as highly active oxidation catalyst.[15]

As for classical zeolites there is a high quest for reducing diffusion limitations and accessibility issues in such oxidation catalysts. The development of purely mesoporous silica-titania has revealed as one approach, yet these materials present a

[a] T. Akkal, Prof. Dr. A. Soualah, Dr. N. Chaouati
Laboratoire de Physique-Chimie des Matériaux et Catalyse (LPCMC), Université de Bejaia, Targa Ouzemmour 06000, Bejaia (Algérie)

[b] T. Akkal, S. Morisset, J. Rousseau, Dr. A. Sachse
Institut de Chimie des Milieux et Matériaux de Poitiers (IC2MP), Université de Poitiers, UMR 7285 CNRS, UFR SFA, Bat. B27, 4 rue Michel Brunet, TSA 51106, 86073 Poitiers, Cedex 9 (France)
E-mail: alexander.sachse@univ-poitiers.fr

Supporting information for this article is available on the WWW under https://doi.org/10.1002/cnma.202200237

© 2022 The Authors. ChemNanoMat published by Wiley-VCH GmbH. This is an open access article under the terms of the Creative Commons Attribution Non-Commercial NoDerivs License, which permits use and distribution in any medium, provided the original work is properly cited, the use is non-commercial and no modifications or adaptations are made.

© 2022 The Authors. ChemNanoMat published by Wiley-VCH GmbH

limited thermal and mechanical stability in comparison to the zeolite-structured counterparts.[16–18]

The hierarchization of TS-1 is hence likely the most suitable solution in order to achieve high catalytic activity and minimized diffusion constrains.[19] Similar post-synthetic approaches as for classical zeolites have been applied for TS-1 and are mainly based on desilication.[20–23] Such alkaline treatments allow for the development of intracrystalline mesopores yet lead to an important variation of the Si/Ti ratio, due to the selective attack of framework silicon and partial collapse of the framework.[24–26] As a function of the treatment mesoporosity of different texture could be introduced as recently reviewed by Yu and coworkers.[27] TS-1 etching using a mixture of HF-NH_4F has recently been reported leading to creation of rather tailored mesopores of 15–30 nm.[28] In this contribution, we firstly investigate the impact of the coherent crystal size and the NH_4F etching on the textural and catalytic properties of TS-1.

Results and discussion

Characterization of the parent TS-1 materials

Two parent TS-1 were prepared using a TPAOH/SiO_2 ratio of 0.40 and 0.26 and named TS-1A and TS-1B, respectively. These present important differences as far as their textural and morphological properties are concerned (Table 1). For both the nitrogen physisorption isotherms are characteristic for microporous materials with micropore volume of 0.2 and 0.19 $cm^3 g^{-1}$ for TS-1A and TS-1B, respectively (Figure 1). The isotherm for TS-1B presents an important nitrogen uptake at elevated relative pressures (>0.85) indicating the presence of interparticular condensation, typical for nanosized zeolites. This is further inferred from the XRD powder patterns that allowed to calculate a CCS of 177 and 95 nm for TS-1A and TS-1B, respectively (Figure 2). These values confirm well the observations from TEM images for which the particle size of TS-1A is roughly twice as high as for TS-1B (Figure 3).

The TPAOH amount in the synthesis only little impacts the Si/Ti ratio, which amounts to 91 and 97 for TS-1A and TS-1B, respectively. The coordination of the Ti sites was investigated through DR-UV/Vis spectroscopy (Figure 4). For both samples a principal band centered at 210 nm was observed, which is characteristic for tetrahedral coordinated framework Ti species.[33] Moreover, a very slight shoulder can be inferred at around 260 nm related to the presence of some titano-oxide oligomers (octa-coordinated Ti).[34] Hence varying the amount of TPAOH in the synthesis little impacts the nature of the active sites.

Characterization of the etched TS-1 materials

Upon etching with the NH_4F solution important textural modifications can be observed for both synthesized materials. A reduction of 0.04 $cm^3 g^{-1}$ of the micropore volume can be observed for both (Table 1). For the hierarchical materials, an important nitrogen uptake in the high relative pressure region at $0.9 \leq P/P_0 \leq 1$ is inferred, which indicates creation of larger mesopores and macropores (Figure 1). This was confirmed from

Table 1. Textural and chemical properties of the prepared TS-1 samples.

Sample	S_{BET}[a] ($m^2 g^{-1}$)	S_{ext}[b] ($m^2 g^{-1}$)	V_{micro}[c] ($cm^3 g^{-1}$)	V_{meso}[d] ($cm^3 g^{-1}$)	D[e] (nm)	CCS[f] (nm)	Si/Ti
TS-1A	473	46	0.2	0.04	150–230	177	91
TS-1AH	447	110	0.16	0.16	140–190	105	87
TS-1B	484	93	0.19	0.14	60–120	95	97
TS-1BH	414	130	0.15	0.2	40–120	49	99

[a, b] Specific (BET) and external surface area; [c, d] Micro and mesoporous volume; [e] Zeolite particle sizes based on TEM images; [f] Coherent Crystal Size.

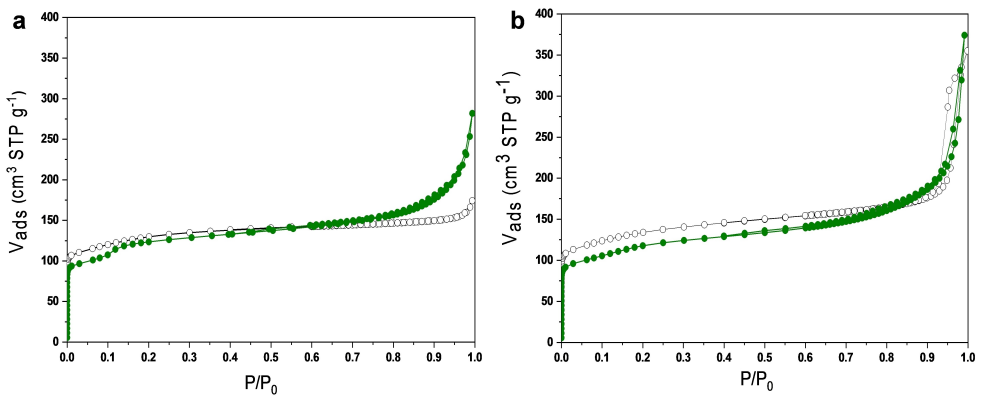


Figure 1. Nitrogen physisorption isotherms at 77 K of the parent TS-1 and etched samples: a) TS-1A (black empty circles) and TS-1AH (green full circles), b) TS-1B (black empty circles) and TS-1BH (green full circles).

© 2022 The Authors. ChemNanoMat published by Wiley-VCH GmbH

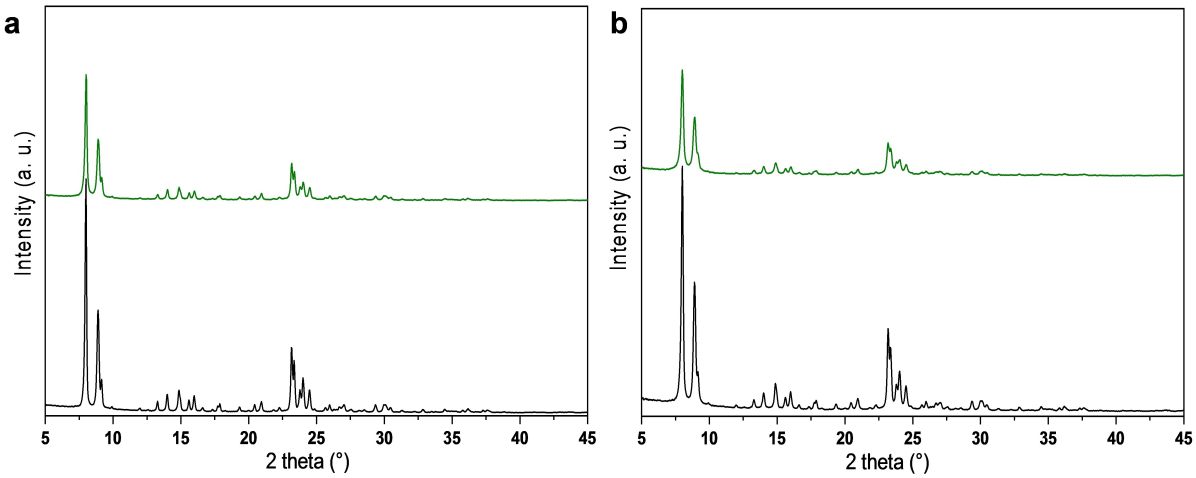


Figure 2. XRD powder patterns of parent TS-1 (black) and etched samples (green) for TS-1A (a) and TS-1B (b).

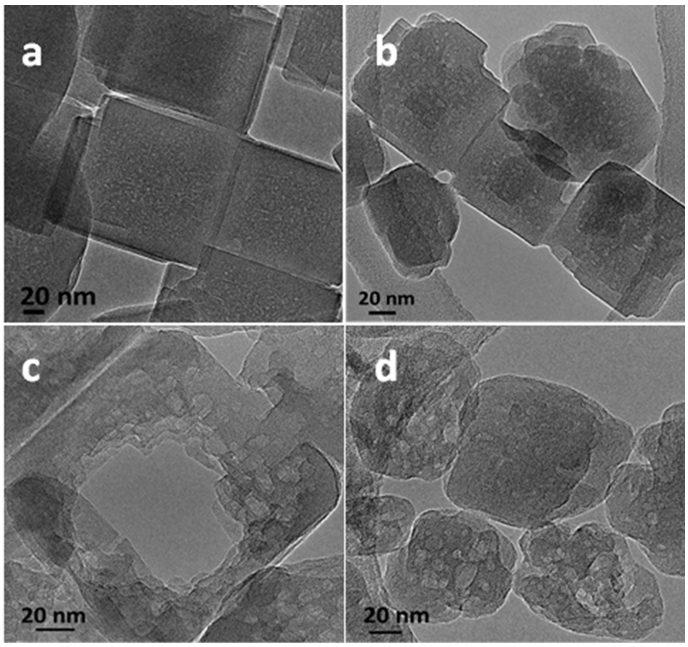


Figure 3. TEM images of parent samples TS-1A (a) and TS-1B (b) and of etched samples TS-1AH (c) and TS-1BH (d).

mercury intrusion (Figure 5). The parent sample (TS-1A) presents intercrystalline void filling down to 100 nm. The intrusion curve thereafter reaches a plateau, indicating the absence of intracystalline macro- and mesopores in the sample. Contrary, the etched sample TS-1AH present mercury intrusion in the range of 100 to 10 nm, indicating the presence of macro- and mesopors of 0.22 $cm^3 g^{-1}$. This value compares well with what was observed from nitrogen physisorption isotherms (Table 1). This finding is confirmed by the TEM images, which present the development of large cavities at the interior of the TS-1AH crystals (Figure 3). By revenge, the developed mesopores are distributed rather homogenously within the crystals for the smaller crystals TS-1BH.

The etching treatment has little impact on the overall crystallinity of the samples and XRD powder patterns present characteristic reflections of the MFI structure (Figure 2). The calculated CCS values indicate reduction of the diffraction domains for both etched samples (Table 1), which confirms the hierarchization of the samples.

As it was previously observed for the Si/Al ratio in silicoaluminate zeolite ZSM-5, the NH_4F etching process little impacts the Si/Ti ratio of the materials, confirming unbiased extraction of Si and Ti (Table 1). The Ti sites moreover remain in framework position during etching as indicated by DR-UV/Vis spectra (Figure 4). This indicates that though important textural modifications upon etching the chemical properties remain unchanged.

The IR spectra of the etched samples resemble those of the parent samples (Figure S1). In the region between 3000 and 4000 cm^{-1}, in which silanol vibrational bands are typically observed, just a very slight band centered at 3730 cm^{-1} can be observed for both parent and hierarchical samples. This finding indicates the presence of little silanols in the parent samples and that the NH_4F treatment does not create a significant amount of silanol defects upon hierarchization.

Catalytic tests

The oxidation of sulfur containing compounds by catalytic oxidation is a sound alternative for the ultra-deep desulfurization of fuels.[34] Such sulfoxidation reactions have further been claimed to present a major interest in the production of fine chemicals.[35]

The catalytic performance of the parent TS-1 and etched samples was compared in the mild oxidation of MPS with hydrogen peroxide (Scheme 1). Figure 6 and Figure S2 present the typical kinetic profiles of the MPS oxidation for the parent and etched samples.[36] The oxidation results in the formation of a sulfoxide (MPSO) and a sulfone ($MPSO_2$). Productivity at 30 min of the MPS conversion is importantly impacted though

© 2022 The Authors. ChemNanoMat published by Wiley-VCH GmbH

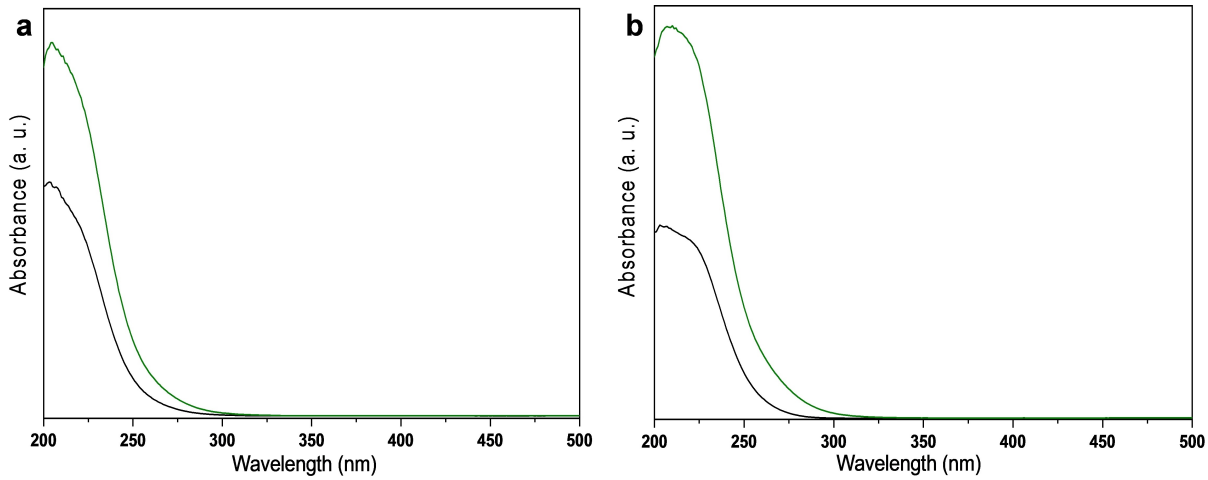


Figure 4. DR-UV-Vis of parent samples (black) and etched samples (green) for TS-1A (a) and TS-1B (b).

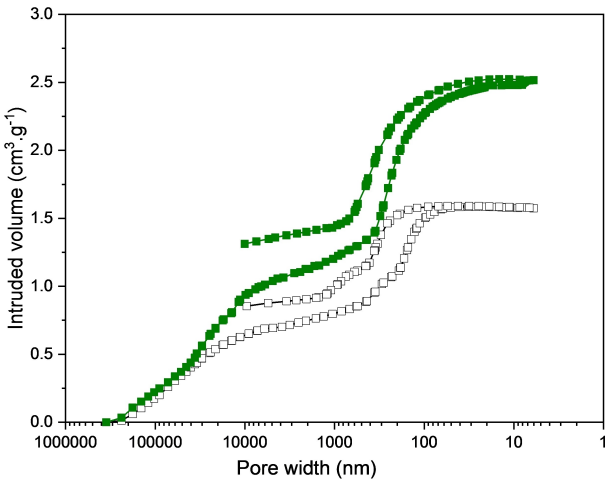
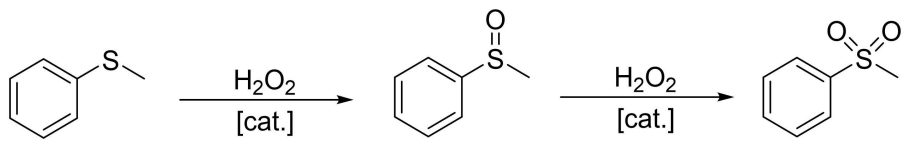


Figure 5. Mercury intrusion and extrusion on TS-1A (black, empty symbols) and TS-1AH (green, full symbols).

etching for the larger zeolite crystals and is 0.68 and 0.93 mmol g^{-1} min^{-1} for TS-1A and TS-1AH, respectively (Table 2). As far the smaller crystals are concerned productivity is higher for both the parent and the etched samples (for which 100% is achieved at 30 min). It is to note that a MPS conversion of 17.4% was observed in a blank test, which is in agreement with the result found in the literature.[37]

The initial velocity was found to be a function of the CCS and increases almost linearly with decreasing CCS until reaching a plateau for CCS values of smaller than 100 nm (Figure 6b), this result is in good agreement with those found in the literature.[3] Hence, it also indicates that the reaction is no longer diffusion limited for materials featuring low CCS values and suggests that the hierarchization of larger crystals has a similar impact as the downsizing of the crystal size.

The CCS further impacts the selectivity of the reaction. As can be observed for the variation of the $MPSO_2$/MPSO ratio at 90% MPS conversion (Table 2). $MPSO_2$/MPSO ratio is highest for the samples featuring larger zeolite crystals (TS-1A) and smallest for the hierarchical nano-crystals (TS-1BH) and amounts to 1.29



Scheme 1. Catalytic sulfoxidation of MPS.

Table 2. The catalytic properties of the parent and treated TS-1.

Sample	V_{init}[a] [mmol g^{-1} min^{-1}]	P_{30}[b] [mmol g^{-1} min^{-1}]	$MPSO_2$/MPSO [at 90% conv.]
TS-1A	0.92	0.68	1.29
TS-1AH	1.4	0.93	1.01
TS-1B	1.55	0.97	1.15
TS-1BH	1.65	1	0.71

[a] Initial velocity; [b] Productivity at 30 minutes reaction.

© 2022 The Authors. ChemNanoMat published by Wiley-VCH GmbH

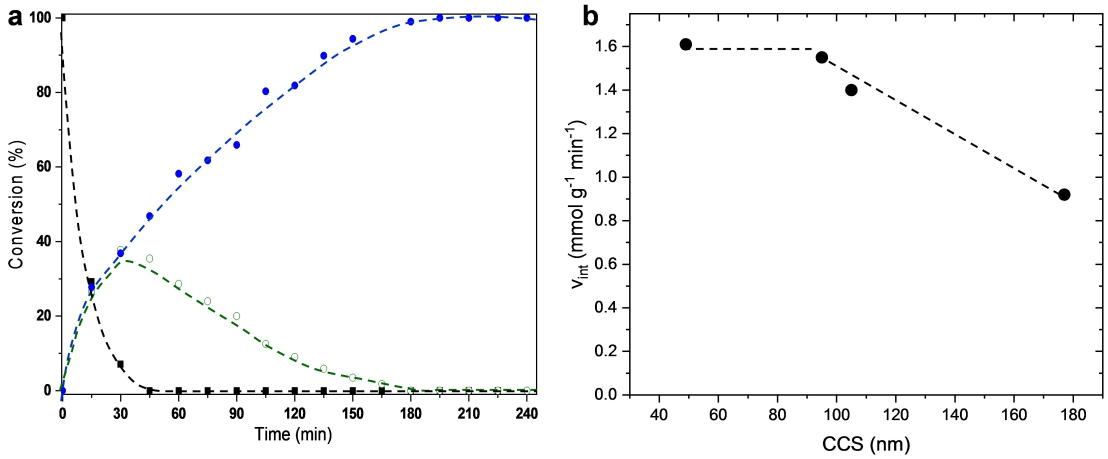


Figure 6. (a) Conversion of MPS (black squares) into MPSO (green empty circles) and $MPSO_2$ (blue full circles) as a function of time for TS-1AH. (b) Initial velocity (v_{Int}) as a function of the Coherent Crystal Size (CCS).

and 0.71, respectively. This indicates that the longer diffusion path length in the TS-1A sample favors the secondary reaction towards the sulfone, whilst for materials presenting shorter diffusion path length (TS-1BH) higher conversion into the mono-oxidized product is achieved, which rapidly diffuses out of micropores. This fosters the observation reported by Martausova et al.[38] who reported a lower $MPSO_2$ selectivity for TS-1 based materials presenting a higher mesopore volume.

Conclusion

TS-1 materials with different crystal sizes could be achieved through adjusting the SiO_2/TPAOH ratio during synthesis. A higher ratio favors the synthesis of smaller crystals with otherwise similar properties as the larger crystals. The impact of a post-synthetic NH_4F treatment on the parent materials was investigated as far as textural and catalytic properties were concerned. The etching process allowed to increase mesopore volume through the generation of larger mesopores. For smaller zeolite crystals the development of more defined mesopores within the crystals was observed. The etching process allowed to maintain Si/Ti ratios, indicating similar chemical properties of parent and etched samples. Both crystal size and hierarchization have shown to importantly impact the catalytic properties in the sulfoxidation of MPS. Initial velocity increased linearly with decreasing CCS until reaching a plateau at 100 nm. Indicating that for TS-1 based materials with CCS smaller than 100 nm the reaction is no longer diffusion limited. The textural properties furthermore play an important role on the catalyst selectivity. For TS-1 with larger CCS higher selectivity towards the di-oxidized product was observed, which indicates the higher degree of secondary reactions for materials featuring longer diffusion path lengths.

Experimental section

Materials

Tetraethylorthosilicate (TEOS, Acro organics, 98%), Titanium butoxide (TBOT Sigma–Aldrich, 97%), tetrapropylammonium hydroxide (TPAOH Sigma–Aldrich, 40%), ammonium fluoride (Sigma–Aldrich, >98%), acetonitrile (Sigma–Aldrich, >99.9%), toluene (Fisher Chemical, >99%), methyl-phenyl sulfide (MPS, Sigma–Aldrich, >99%) and H_2O_2 (Sigma–Aldrich, 30% in water) were used as received.

Synthesis of parent TS-1 materials

TS-1 materials with two different particle size were synthesized using an adapted procedure from van der Pol et al.[29] In a typical procedure, TEOS and TBOT were stirred at 308 K for 2 h in a 250 ml flat-bottomed flask. The mixture was thereafter placed in an ice bath for 15 min and TPAOH was added dropwise under vigorous stirring and kept at this temperature for 90 minutes. The mixture was then heated at 353 K for 4 h until complete evaporation of ethanol. Finally, the pH of the gel was adjusted to 12.2 by adding deionized water. The molar ratio of the synthesis gel was 1TEOS:0.01TBOT:xTPAOH:H_2O, with x = 0.40 and 0.26 for TS-1A and TS-1B, respectively. The gel was then transferred into a Teflon stainless steel autoclave and crystallized at 443 K for 48 h under rotation (120 rpm). The synthesized materials were recovered by centrifugation, washed to neutral pH, dried at 80 °C overnight, and finally calcined at 550 °C for 6 hours under air using a heating rate (1 °C min^{-1}).

NH_4F treatment

0.5 g of TS-1A or TS-1B were added to 10 g of a 40 wt% aqueous NH_4F solution at 50 °C under stirring during 90 minutes in a closed vessel. After filtration and washing with deionized water (four times), the recovered solids were dried at 80 °C overnight, and then calcined at 550 °C for 4 h under air (1 °C min^{-1}). The resulting samples were named TS-1AH and TS-1BH.

© 2022 The Authors. ChemNanoMat published by Wiley-VCH GmbH

Characterization

X-ray powder diffraction patterns were recorded on a PANalytical EMPYREAN X-ray diffractometer (operating at 45 Kv–40 mA), using CuKα radiation (1.54059 Å), with a scanning rate 0.008° min^{-1}. Coherent crystal size (CCS) was calculated using Williamson-Hall analysis by using equation 1.[30]

$$\cos\,\theta\,\beta_T = \frac{K\lambda}{CCS} + 4\,\varepsilon\,\sin\,\theta \quad (1)$$

DRUV-Vis spectra were collected from 200 to 800 nm using a UV-Visible-PIR Cary 5000 Varian – Agilent with $BaSO_4$ as a reference. Nitrogen physisorption isotherms were measured on a Micrometrics 3Flex instrument at 77 K. Prior to the analysis, all samples were degassed at 623 K for 10 h. The specific surface areas (S_{BET}) was calculated using the Brunauer–Emmett–Teller (BET) equation on the linear zone of the BET plot using Rouquerol criterion.[31] Microporous volume was determined from *t*-plot using the reference described by Batonneau-Gener et al.[32] The total pore volume was taken at $P/P_0 = 0.96$, the mesopore volume was estimated from the difference of the total and micropore volume. Mercury porosimetry analysis was performed using a Micromeritics AUTOPORE IV 9500. The elemental composition of materials was determined by the use of inductively coupled plasma atomic emission spectroscopy (ICP-OES), using a Perkin Elmer Optima 2000DV instrument. Transmission Electron Microscopy (TEM) images were recorded on a JEOL 2100 instrument (operating at 200 kV with a LaB_6 source and equipped with a Gatan Ultra scan camera).

Catalytic tests

In a 50 mL three-necked round-bottom flask immersed in an oil bath under strong stirring (1000 rpm) at 60 °C a solution of 1.5 mmol MPS, 15 mL acetonitrile and 1.5 mmol toluene (used as internal standard) was prepared. 3 mmol H_2O_2 (30%) was added and immediately thereafter 50 mg of activated catalyst was dispersed in the mixture. The blank test was performed under the same operating conditions but without the addition of a catalyst. The reaction was followed through sampling of the reaction and analyzed using an Agilent 7820 A gas chromatograph equipped with a DB-5 (30 m × 0.25 mm, 0.25 μm) capillary column and FID detector. The conversion, productivity (P) and initial velocity were calculated using equations 2, 3 and 4, respectively.

$$\text{Conv. (MPS)} = \frac{n_0(\text{MPS}) - n_t(\text{MPS})}{n_0(\text{MPS})}\,100 \quad (2)$$

$$P_t = \frac{n_t(\text{MPS})\ \text{Conv.(MPS)}}{t\ m}\,0.01 \quad (3)$$

$$v_{int} = a\ \frac{n_0(\text{MPS})}{m}\ 0.01 \quad (4)$$

Where *t*, *m*, and *n* represent the time (min), used catalyst mass (g) and moles products or reactants respectively. *a* represents the slope of the variation of the MPS conversion as a function of time taken between 0 and 15 minutes.

Supporting Information

Kinetic profiles of MPS conversion for TS-1A, TS-1B and TS-1BH are available as supporting information.

Acknowledgements

The authors acknowledge financial support from the European Union (ERDF) and "Région Nouvelle Aquitaine". The authors further acknowledge financial support from PHC TASSILI program #43773VB.

Conflict of Interest

The authors declare no conflict of interest.

Data Availability Statement

The data that support the findings of this study are available from the corresponding author upon reasonable request.

Keywords: zeolites · hierarchical · titanosilicate · TS-1 · desulfurization · oxidation · ammonium fluoride

[1] J. Perez-Ramirez, C. H. Christensen, K. Egeblad, C. H. Christensend, J. C. Groene, *Chem. Soc. Rev.* **2008**, *37*, 2530.
[2] M. Hartmann, A. G. Machoke, W. Schwieger, *Chem. Soc. Rev.* **2016**, *45*, 3313.
[3] G. Bellussi, R. Millini, in *Structure and Reactivity of Metals in Zeolite Materials* (Eds. J. Pérez Pariente, M. Sánchez-Sánchez), Springer, **2017**, pp. 1–52.
[4] C. S. Cundy, J. O. Forrest, R. J. Plaisted, *Microporous Mesoporous Mater.* **2003**, *66*, 143.
[5] G. Froment, *J. Catal.* **1990**, *124*, 39.
[6] S. Mintova, J. Grand, V. Valtchev, *C. R. Chim.* **2016**, *19*, 183.
[7] M. V. Opanasenko, W. J. Roth, J. Čejka, *Catal. Sci. Technol.* **2016**, *6*, 2467.
[8] A. Sachse, J. García-Martínez, *Chem. Mater.* **2017**, *29*, 3827.
[9] R. Chal, C. Gérardin, M. Bulut, S. van Donk, *ChemCatChem* **2011**, *3*, 67.
[10] A. Feliczak-Guzik, *Microporous Mesoporous Mater.* **2018**, *259*, 33.
[11] Z. Qin, M. Georgian, J. P. Gilson, M. Jaber, K. Bozhilov, *Angew. Chem. Int. Ed.* **2016**, *128*, 15273.
[12] Z. Qin, L. Pinard, M. A. Benghalem, T. J. Daou, G. Melinte, O. Ersen, S. Asahina, J.-P. Gilson, V. Valtchev, *Chem. Mater.* **2019**, *31*, 4639.
[13] L. Nemeth, S. R. Bare, *Adv. Catal.* **2014**, *57*, 1.
[14] M. Taramasso, G. Perego, B. Notari, US Patent No. 4,410,501, **1983**.
[15] U. Romano, A. Esposito, F. Maspero, C. Neri, M. G. Clerici, *Stud. Surf. Sci. Catal.* **1990**, *55*, 33.
[16] J. Vernimmen, M. Guidotti, J. Silvestre-Albero, E. O. Jardim, M. Mertens, O. I. Tendeloo, R. Psaro, F. Rodriguez-Reinoso, V. Meynen, P. Cool, *Langmuir* **2011**, *27*, 3618.
[17] P. Wu, H. Xu, L. Xu, Y. Liu, M. He, in *MWW-Type Titanosilicate*, Springer, **2013**, pp. 9–34.
[18] A. Sachse, V. Hulea, K. L. Kostov, N. Marcotte, M. Yu Boltoeva, E. Belamie, B. Alonso, *Chem. Commun.* **2012**, *48*, 10648.
[19] J. Přech, R. E. Morris, J. Čejka, *Catal. Sci. Technol.* **2016**, *6*, 2775.
[20] Y. Wang, M. Lin, A. Tuel, *Microporous Mesoporous Mater.* **2007**, *102*, 80.
[21] S. T. Tsai, P.-Y. Chao, T.-C. Tsai, I. Wang, X. Liu, X.-W. Guo, *Catal. Today* **2009**, *148*, 174.
[22] X. F. Zhang, J. Yao, X. Yang, *Microporous Mesoporous Mater.* **2017**, *247*, 16.
[23] G. Lv, F. Wang, X. Zhang, B. P. Binks, *Langmuir* **2018**, *34*, 302.

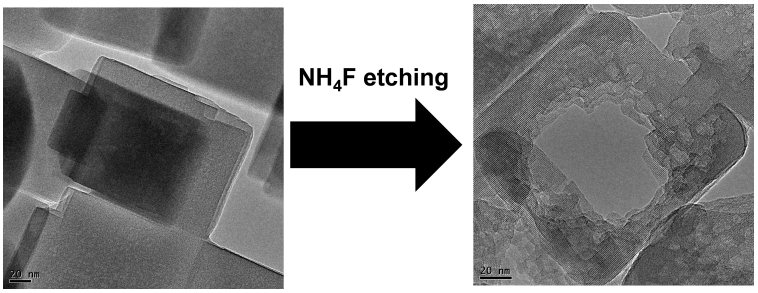
© 2022 The Authors. ChemNanoMat published by Wiley-VCH GmbH

[24] A. Silvestre-Albero, A. Grau-Atienza, E. Serrano, J. García-Martínez, J. Silvestre-Albero, *Catal. Commun.* **2014**, *44*, 35.
[25] J. Tekla, K. A. Tarach, Z. Olejniczak, V. Girman, K. Góra-Marek, *Microporous Mesoporous Mater.* **2016**, *233*, 16.
[26] P. Y. Chao, S.-T. Tsai, T.-C. Tsai, J. Mao, X.-W. Guo, *Top. Catal.* **2009**, *52*, 185.
[27] R. Bai, Y. Song, R. Bai, J. Yu, *Adv. Mater. Interfaces* **2021**, *8*, 2001095.
[28] S. Du, X. Chen, Q. Sun, N. Wang, M. Jia, V. Valtchev, J. Yu, *Chem. Commun.* **2016**, *52*, 3580.
[29] A. J. H. P. van der Pol, A. J. Verduyn, J. H. C. van Hooff, *Appl. Catal. A* **1992**, *92*, 113.
[30] N. Linares, A. Sachse, E. Serrano, A. Grau-Atienza, E. D. O. Jardim, J. Silvestre-Albero, M. A. L. Cordeiro, F. Fauth, G. Beobide, O. Castillo, J. García-Martínez, *Chem. Mater.* **2016**, *28*, 8971.
[31] J. Rouquerol, P. Llewellyn, F. Rouquerol, *Stud. Surf. Sci. Catal.* **2007**, *170*, 49.
[32] I. Batonneau-Gener, A. Sachse, *J. Phys. Chem. C* **2019**, *123*, 4235.
[33] J. Su, G. Xiong, J. Zhou, W. Liu, D. Zhou, G. Wang, X. Wang H Guo, *J. Catal.* **2012**, *288*, 1.
[34] A. Sachse, V. Hulea, K. L. Kostov, E. Belamie, B. Alonso, *Catal. Sci. Technol.* **2015**, *5*, 415.
[35] Z. Ismagilov, S. Yashnik, M. Kerzhentsev, V. Parmon, A. Bourane, F. M. Al-Shahrani, A. A. Hajji, O. R. Koseoglu, *Catal. Rev.* **2011**, *53*, 199.
[36] R. A. Sheldon, *Stud. Surf. Sci. Catal.* **1991**, *59*, 33.
[37] Z. Kang, G. Fang, Q. Ke, J. Hu, T. Tang, *ChemCatChem* **2013**, *5*, 2191.
[38] I. Martausov, D. Spustova, D. Cvejn, A. Martaus, Z. Lacny, J. Prech, *Catal. Today* **2019**, *324*, 144.

Manuscript received: May 19, 2022
Revised manuscript received: August 15, 2022
Version of record online: ■■, ■■■

© 2022 The Authors. ChemNanoMat published by Wiley-VCH GmbH

RESEARCH ARTICLE



*T. Akkal, Prof. Dr. A. Soualah, S. Morisset, J. Rousseau, Dr. N. Chaouati, Dr. A. Sachse**

1 – 8

Hierarchical TS-1 Through Ammonium Fluoride Etching

Ammonium fluoride etching of TS-1 allows for the unbiased leaching of Si and Ti and to the generation of large mesopores that efficiently allow to reduce the diffusion path length in catalysis.